

Automated extraction of single H atoms with STM: tip state dependency

This content has been downloaded from IOPscience. Please scroll down to see the full text.

2017 Nanotechnology 28 075302

(<http://iopscience.iop.org/0957-4484/28/7/075302>)

View [the table of contents for this issue](#), or go to the [journal homepage](#) for more

Download details:

IP Address: 128.243.2.140

This content was downloaded on 16/01/2017 at 14:46

Please note that [terms and conditions apply](#).

You may also be interested in:

[Single-atom reversible recording at roomtemperature](#)

U J Quaade, K Stokbro, R Lin et al.

[Manipulation of polyatomic molecules with the STM: chlorobenzene/Si\(111\)-\(7times7\)](#)

P A Sloan and R E Palmer

[Silicon-basedmolecular nanotechnology](#)

M C Hersam, N P Guisinger and J W Lyding

[Controllable dissociations of PH3 molecules on Si\(001\)](#)

Qin Liu, Yanhua Lei, Xiji Shao et al.

[Vibrational-Energy Redistribution in Single-Atom Manipulation by Scanning Tunneling Microscope](#)

Qiang Shi, Dehuan Huang and Qingshi Zhu

[Nanoscale patterning and selective chemistry of silicon surfaces by ultrahigh-vacuum scanning tunneling microscopy](#)

J W Lyding, T-C Shen, G C Abeln et al.

[Molecular and atomic manipulation mediated by electronic excitation of the underlying Si\(111\)-7x7 surface](#)

Kristina R Rusimova and Peter A Sloan

[Lithography and doping in strained Si towards atomically precise device fabrication](#)

W C T Lee, S R McKibbin, D L Thompson et al.

[Atomic-scale patterning of hydrogen terminated Ge\(001\) by scanning tunnelingmicroscopy](#)

G Scappucci, G Capellini, W C T Lee et al.

Automated extraction of single H atoms with STM: tip state dependency

Morten Møller¹, Samuel P Jarvis^{1,4}, Laurent Guérinet², Peter Sharp¹, Richard Woolley³, Philipp Rahe¹ and Philip Moriarty¹

¹School of Physics and Astronomy, University of Nottingham, Nottingham, NG7 2RD, UK

²Institut National des Sciences Appliquées de Toulouse, 135, Avenue de Rangueil - 31077, Toulouse, Cedex 4 France

³Quantulus Technology Ltd, Fairway Road, Shepshed, Leicestershire LE12 9DS, UK

⁴Physics Department and Materials Science Institute, Lancaster University, Lancaster LA1 4YB, UK

E-mail: Philip.Moriarty@nottingham.ac.uk

Received 16 September 2016, revised 1 November 2016

Accepted for publication 2 November 2016

Published 11 January 2017



CrossMark

Abstract

The atomistic structure of the tip apex plays a crucial role in performing reliable atomic-scale surface and adsorbate manipulation using scanning probe techniques. We have developed an automated extraction routine for controlled removal of single hydrogen atoms from the H:Si(100) surface. The set of atomic extraction protocols detect a variety of desorption events during scanning tunneling microscope (STM)-induced modification of the hydrogen-passivated surface. The influence of the tip state on the probability for hydrogen removal was examined by comparing the desorption efficiency for various classifications of STM topographs (rows, dimers, atoms, etc). We find that dimer-row-resolving tip apices extract hydrogen atoms most readily and reliably (and with least spurious desorption), while tip states which provide atomic resolution counter-intuitively have a lower probability for single H atom removal.

Keywords: scanning probe microscopy, STM, atomic manipulation, hydrogen desorption, tip state


(Some figures may appear in colour only in the online journal)

1. Introduction

In scanning probe microscopy (SPM), the ability to image and perform atomic and molecular manipulation has unsurprisingly been shown to be critically dependent on the state of the tip. Since their invention in the eighties, these instruments have been invaluable for investigating and manipulating surfaces and adsorbates at the atomic scale. An especially important class of atomic manipulation tool is available via the scanning tunnelling microscope (STM), which has the capability to perform hydrogen resist lithography on H:Si(100) surfaces [1–4] with single atom specificity [5]. This technique has been used to fabricate not only prototype but functional electronic devices, including quantum dots [6, 7],

conducting wires [8], and single atom transistors [9], and has been elegantly exploited to generate and manipulate artificial molecular orbitals (arising from dangling bond (DB) interactions) at the Si(100) surface [10]. One of the main advantages of STM-induced depassivation of this type is that it allows atomic scale imaging in concert with the patterning process, thus offering a high degree of operational control.

With the ultimate goal of autonomously fabricating atomic scale structures, we have implemented the following protocols. In order to automate and control the H:Si(100) patterning process with single-atom specificity, a feedback-controlled lithography (FCL) approach based on the technique developed by Lyding *et al* [5] was implemented. By actively monitoring the STM feedback signal and controlling the desorption parameters during patterning, individual atoms can selectively and ‘autonomously’ be desorbed. Similar protocols for automated atom-precision lithography have been developed by Randall and co-workers at Zyvex Labs

 Original content from this work may be used under the terms of the [Creative Commons Attribution 3.0 licence](https://creativecommons.org/licenses/by/3.0/). Any further distribution of this work must maintain attribution to the author(s) and the title of the work, journal citation and DOI.

[11]; the resulting control system, ZyVector, is now commercially available. We show that for the variant of the FCL technique we have adopted, robust detection of single desorption events is possible. More importantly, the automation protocols we have developed enable the systematic generation and analysis of thousands of hydrogen desorption events, which in turn have provided key insights into the role that the atomistic structure of the tip apex plays in the extraction process.

The STM desorbs hydrogen atoms through inelastic electron scattering mechanisms [2, 3, 12, 13]. At conditions of relatively high current and low electron energy tunneling, such as those used in our experiments, the desorption mechanism involves multi-quantum vibrational excitations of the Si–H bond [2, 12, 14–16]. (At higher electron energies electrons possess sufficient energy to directly promote an electron from the Si–H bonding state to its corresponding antibonding orbital.) Previous studies have demonstrated that the basic desorption process involves only a single Si–H bond which is vibrationally excited by tunnelling electrons [2, 17]. Although the H:Si(100) surface [18–21], and the desorption mechanism [2, 3, 12, 13], have been studied extensively, the influence of the tip state on the desorption process has hitherto not been examined in any depth. For example, while the desorption efficiency has been analyzed for different bias and current parameters [22], these experiments did not take the state of the tip into account. Theoretical studies of atomic force microscope-based atomic manipulation [23–25] clearly, and unsurprisingly, show that the atomistic detail of the tip termination plays a crucial role in the process. (Unlike STM-tip-induced desorption, however, AFM-based manipulation on Si(100) surfaces is mediated by direct chemical interaction.)

In this work, we examine the influence of the atomistic structure of the tip apex on the desorption efficiency for STM-induced H atom extraction. Through a detailed, systematic analysis of thousands of H atom desorption events, we show that tips that produce row-resolved STM topographs yield single atom desorption events more reliably than tip apices which generate either dimer-resolved or atomically-resolved images. Moreover, row-resolving tip apices also generate the smallest number of spurious desorption events. (This dependence of spurious hydrogen desorption on the tip state was postulated previously by Ballard *et al* [26]. Here we provide strong evidence to support their hypothesis.) This sensitivity of H atom extraction to the precise atomistic structure of the tip is a critical factor in ensuring the reproducibility and reliability of atomic scale engineering of hydrogen-passivated semiconductor surfaces.

2. Methods

Silicon samples cut from Si(100) wafers (n-type, 6 m Ω cm) were used throughout our experiments. Samples were prepared in an ultra-high vacuum (UHV) chamber with a base pressure of 5×10^{-11} mbar or less. Low base pressures were obtained by baking the UHV chamber at 145 °C twice over

prolonged periods (three to four days). The samples were outgassed for a minimum of 12 h at 600 °C. Clean Si(100) 2×1 samples were obtained by flash heating to 1150 °C for 10 s, followed by gradual cooling from 900 °C (at a rate of ~ 1 °C s $^{-1}$) to room temperature. For hydrogen passivation, the sample was exposed to atomic hydrogen, which is obtained by cracking molecular hydrogen using a Specs GmbH thermal gas cracker, positioned approximately 10 cm from the sample. H $_2$ was introduced into the chamber, through the gas cracker, until a pressure of 1×10^{-6} mbar was reached. The sample was exposed for 1 min (i.e. 60 Langmuirs). During exposure, the sample was held at a temperature of 360 ± 20 °C in order to achieve hydrogen-terminated Si(100)- 2×1 surfaces and avoid other reconstructions (such as (3×1)).

Measurements were performed on an Omicron variable-temperature (VT) STM-AFM system with a MATRIX control system. All experiments were performed at room temperature (RT). Tungsten tips were used for both STM imaging and hydrogen extraction. These were electrochemically etched and subsequently annealed to ≤ 1000 °C in the UHV chamber, in order to remove the oxide layer, before STM use. In order to randomize our statistics, the tip apex was routinely prepared during STM imaging using voltage pulsing and controlled tip crashing. Atom tracking [27] was used to eliminate drift during all automated extraction routine trials, unless otherwise stated. All STM images presented in this article were obtained with a sample bias voltage of 1.6 V and a constant current of 10 pA.

3. Results

Figure 1 shows a flow diagram of the automated DB generation routine. Upon activation of the automation routine, the tip was positioned at the desired location for atom extraction, and the initial parameters were subsequently changed to the desired desorption parameters V_D , I_D . Upon reaching the desorption parameters, the $Z(t)$ feedback signal is then used to monitor in real-time for a jump in Z . A threshold jump height of 0.3 Å was found most suitable for detecting a desorption event, as higher thresholds potentially lead to desorption events not being detected, while smaller thresholds increase the probability of false detections. If a step in Z ($Z_{\text{step}} \geq 0.3$ Å) is detected, the desorption parameters subsequently rebound to the initial scan parameters. For step detection, a 10 ms integration time was found to be most appropriate as larger integration times could lead to multiple desorption events. Figure 2 shows a typical z -jump detection event, including the full voltage- and current-ramp-related changes in the z position, for generation of a single DB.

The automated extraction routine can be used for arbitrary patterning with high fidelity as shown in figure 3, where the extraction routine is used to atomically generate a 4×4 array of DBs. The reliability of the automated extraction routine was evaluated by comparing step detections from the routine with the true outcome as observed from STM imaging. The results are plotted in figure 4, for 1126 trials. For

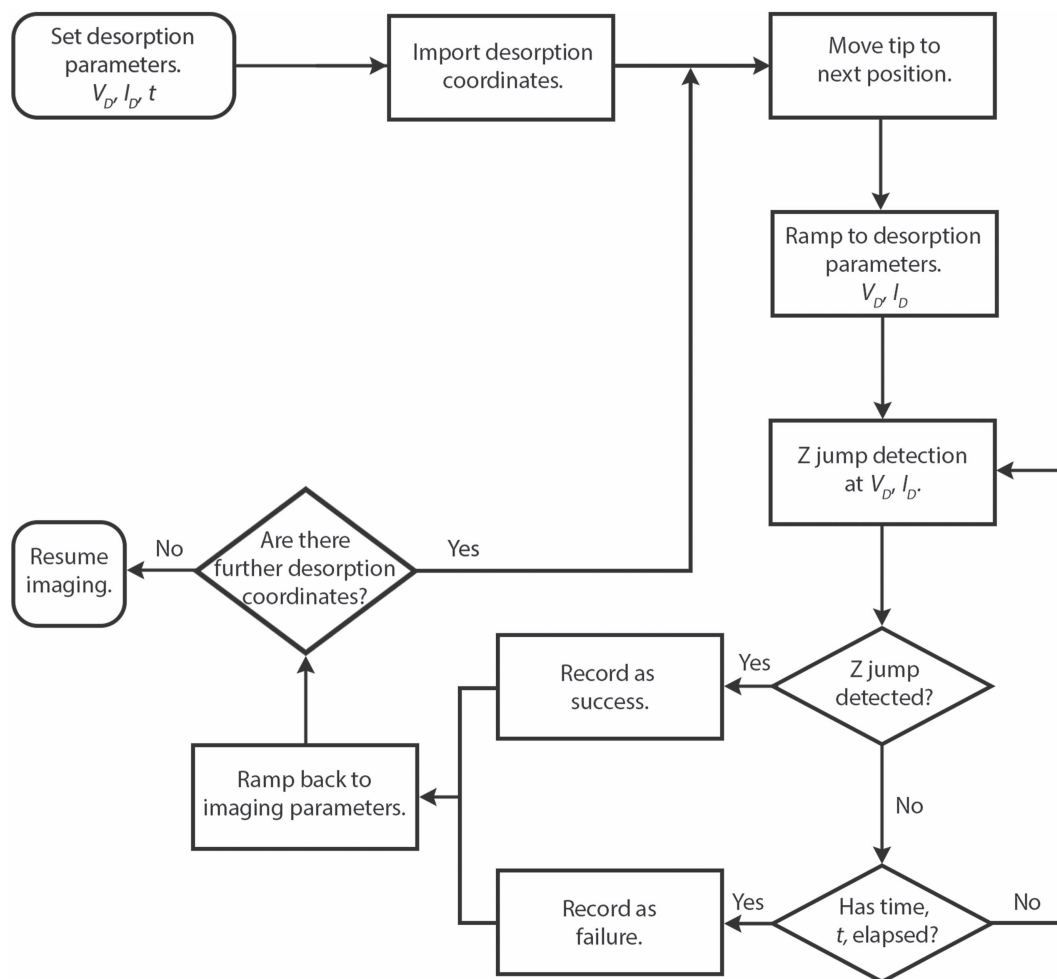


Figure 1. Flow diagram showing implementation of automated DB generation. The tip is initially positioned using predetermined desorption parameters and coordinates, followed by a change from scanning conditions to desorption parameters (V_D , I_D , t). The feedback signal, $Z(t)$, was then monitored in real time. Following detection of a jump in Z , or an elapsed time t , the parameters were subsequently restored to the imaging conditions. The desorption procedure was then repeated for all input coordinates.

each trial, the extraction routine is run for 60 s using similar desorption parameters. Desorption events are classified based on whether *any* desorption occurs directly underneath the tip (primary) or if *none* occurs directly underneath the tip. Desorption events with either an uncertain number, or more than four DBs generated, are collectively called clusters. We find that our step detection algorithm reliably detects any type of desorption, whether they occur directly underneath the tip (primary) or not, but elsewhere (secondary). Single atom extraction events are detected with a 90% accuracy. Other unwanted events, such as multiple desorption events, or secondary desorptions, are similarly reliably detected. Unfortunately, the automated desorption algorithm does, unavoidably, occasionally register false jumps. This is mainly due to a combination of noise in Z and a low Z -threshold value. As discussed below, the tip state plays a key role in triggering false detection events.

It is well known that the structure of the tip can change during a desorption event as a result of tip–surface interactions [4]. To investigate the desorption efficiency under practical conditions, data containing tip changes *during* desorption were not excluded. Only a small subset (8.9%) of the

total number of trials involved tip-state changes. All tip imaging states were classified based on the image observed prior to desorption. Only data that could not be classified into the four tip imaging states (row, dimer, atom, asymmetric) *prior to desorption* were excluded (constituting 1.7% of trials).

The dependence of the desorption efficiency on the atomistic structure of the tip apex was determined by grouping the tip states into a set of broad classes. Figures 5(a)–(d) show a selection of observed tip states, and their respective grouping into the following classes: (a) rows, (b) dimers, (c) atomic, and (d) asymmetric.

The desorption efficiency is plotted in figure 6 as a function of voltage, for each respective type of observed tip states ((a) row, (b) dimer, (c) atomic, and (d) asymmetric). All tip states that could be classified into these groupings (2023 out of 2074 trials) were included in our analysis. Each data value in the figure corresponds to an experimental run of the automated extraction routine. In order to gauge the desorption efficiency as a function of voltage, all data were acquired by keeping the desorption parameters fixed (1.2 nA, V_{fixed}) for a given bias for the same amount of time (60 s). All

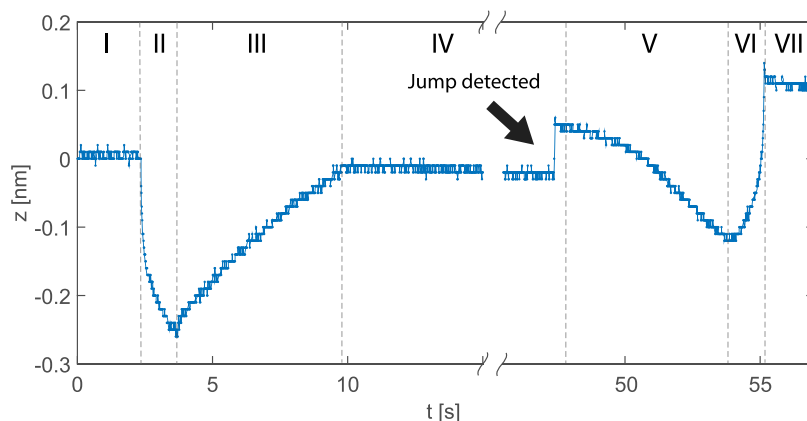


Figure 2. The feedback (z) for automated DB generation performed at fixed position. (I) moved to position, (II) ramping I_D , (III) ramping V_D , (IV) Z jump detection at I_D , V_D , (V) ramp V_D back to imaging parameter, (VI) I_D , and (VII) reached imaging parameters.

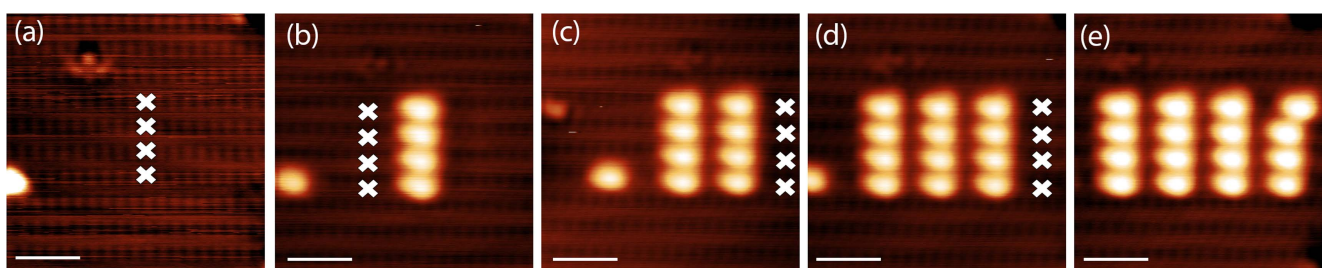


Figure 3. Successive single desorption events showing dangling bond formation using automated extraction routine. In images (a)–(d), each white ‘x’ represents the coordinates which were input to the H extraction algorithm. Sequential application of the algorithm produced the 4×4 dangling bond array shown in (e). $V_D = 2$ V, $I_D = 250$ – 800 pA.

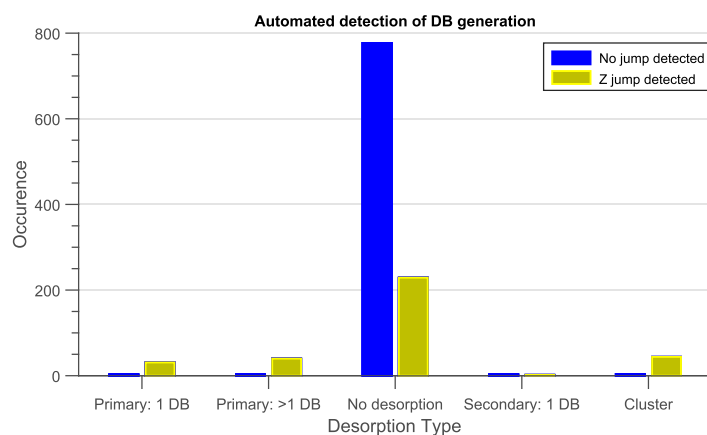


Figure 4. Detection efficiency for different desorption types using the automated detection algorithm. Here, *primary* refers to the generation of at least one dangling bond directly underneath the tip (preselected desorption coordinate), while *secondary* is used when *no* desorption occurs underneath the tip (but occurs elsewhere). *Clusters* refers to the generation of more than four dangling bonds (DBs) or an indistinguishable number of DBs.

experimental trials performed at each voltage value (V_{fixed}) were therefore normalized to 1. Data where false detections occurred before 60 s were excluded.

We observe that the onset of desorption follows the general tip classification rule: $V_{\text{row}} \geq V_{\text{dimer}}$, $V_{\text{asymmetric}} \geq V_{\text{atomic}}$ for a given bias, respectively. This translates into a desorption probability that follow the same rule: $P_{\text{row}} \geq P_{\text{dimer}}$, $P_{\text{asymmetric}} \geq P_{\text{atomic}}$. These results are further corroborated by

similar findings using other STM tips and using different FCL automation routines (not included).

4. Discussion

Our findings show that row-resolved tip states produce a single desorption event more reliably than other tip states, and

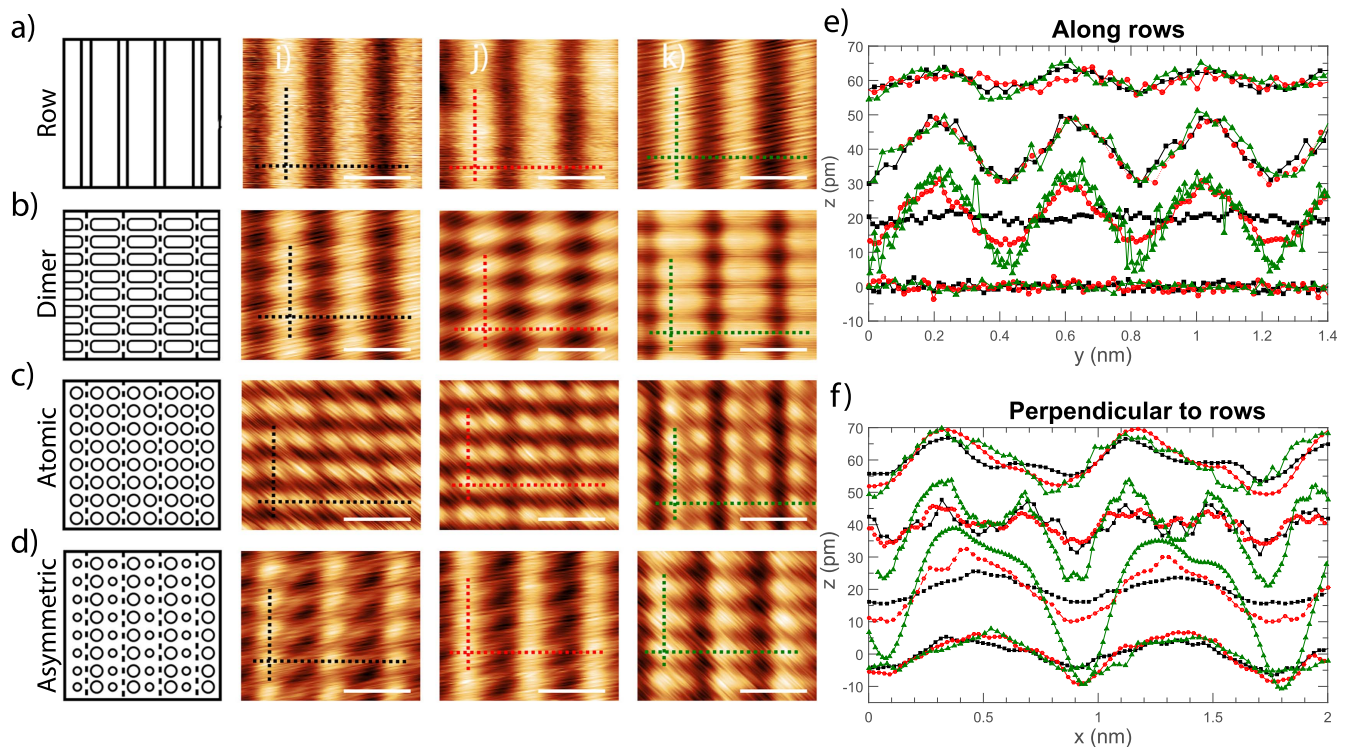


Figure 5. Classification of tip imaging state into: (a) rows, (b) dimers, (c) atoms, and (d) asymmetrical. The STM images have been rotated to align the direction of dimer rows. Line profiles (e) along and (f) perpendicular to rows from positions indicated in (a)–(d). Note that some of the profiles have been shifted by an offset of 20 pm for clarity. Scale bars correspond to 0.77 nm (i.e. the dimer row separation on Si(100)).

that other unwanted reactions (such as producing clusters) are less likely for the row-resolving tip apex than for other states. The reason for this remains as yet unclear but an obvious candidate explanation relates to the density of states of the tip apex. Although the STM image contrast mechanism has been investigated for bare [28, 29], and passivated Si(100) surfaces [30, 31], this has been in the context of the density of states and band structure of the substrate; the influence of the atomistic structure of the tip on the contrast mechanism has not yet been investigated.

For our desorption conditions (electron energies <4 eV), the dominant desorption mechanism is attributed to inelastic scattering of the tunneling electrons with the Si–H bond [2, 12]. Using this model, the tunneling probability is dependent on several factors, including, of course, the local density of states (LDOS) of the tip. It is therefore reasonable to speculate that for the H:Si(100) surface, tip states producing row-like STM topographs might have a greater density of states (in the energy window defined by the tip–sample bias) than other classes of tip apex. This will directly affect the available flux of electrons and, thus, the desorption probability.

Although early theoretical studies suggested that while the electric field under the tip is insufficient to directly induce H atom desorption, it could nonetheless play a significant role via spatial localization of the excitation [14] due to a Stark effect. However, subsequent experiments, where neighboring hydrogen atoms were extracted, show that interdimer

extraction is more favorable than intradimer extraction, suggesting that the presence of an electric field does not play a significant role in the desorption process [17]. Our results support these latter findings. Moreover, we find that the distribution of different types of neighboring desorption events is also tip-state dependent, where intradimer desorption occurs more frequently for atomically resolved STM topographs. We are planning a systematic combined density functional theory (DFT)-non-equilibrium Greens function study in order to elucidate the origin of the higher desorption efficiency of the row-resolving class of tip apices (and to ascertain the extent to which the H desorption process is mediated by the structure and density of states of the tip apex).

Our findings have shown that extracting single H atoms is best achieved for row-resolving tip imaging states and low bias voltages. Additionally, at these conditions, undesirable side effects such as multiple or secondary desorptions are also minimized. The low bias voltage probably plays a significant role in limiting the number of unwanted desorption events as the yield is highly dependent on the the bias voltage and electron dosage [2–4]. Based on our findings we conclude that the best strategies for controlling the automated patterning process can be obtained by (I) carefully selecting the proper tip geometries for desorption, (II) controlling the desorption yield (affected by desorption parameters, tip–sample distance), and (III) through reliable detection of H extraction by either minimizing/excluding noise influences or improving the step detection algorithm.

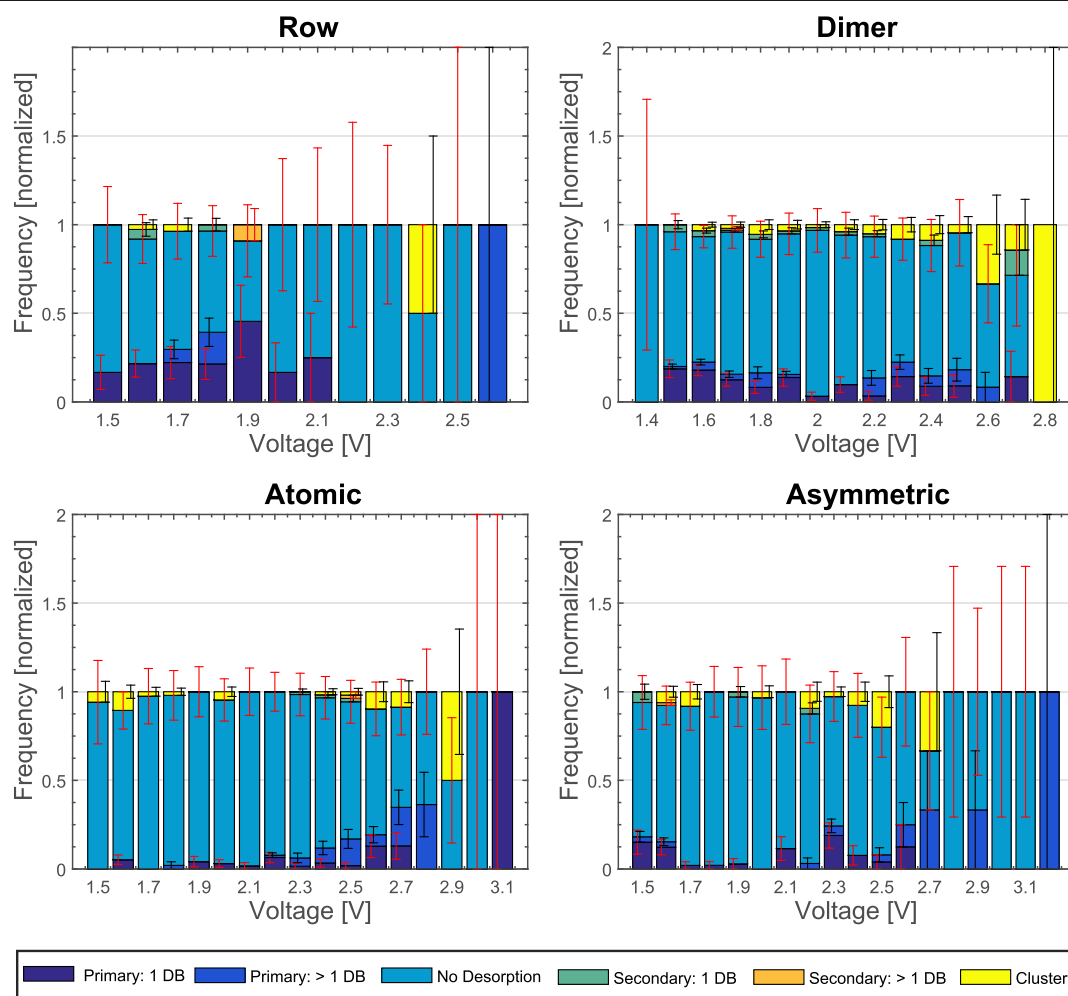


Figure 6. Desorption frequency for each desorption type as a function of voltage for different tip imaging states. Each data point corresponds to a run of the automation routine over a fixed voltage value V_{fixed} (normalized to 1 for each V_{fixed} value) for 60 s.

5. Conclusions

We have implemented an automated extraction routine capable of implementing and detecting single H atom desorption from H:Si(100) surfaces with high reliability. The routine was used to examine the influence of the tip state on the desorption efficiency by desorbing atoms using fixed desorption parameters, for a fixed time. Tip states were classified into four broad types: row-resolving, atom-resolving, dimer-resolving, and ‘asymmetric’ and their desorption efficiencies compared. We find that tips that produced row-resolved STM topographs desorb H atoms most efficiently. Our results are used to propose strategies for controlling the accuracy of single H atom extraction. Future work will focus on elucidating the origin of the tip state dependency of the desorption process via a combined density functional theory (DFT)-Green’s function approach.

Acknowledgments

This work was supported by the Engineering and Physical Sciences Research Council [grant numbers EP/G007837/1, EP/J500483/1], PM thanks the Engineering and Physical

Sciences Research Council for a Leadership Fellowship award which supported some of this work (EP/G007837/1) and SPJ was funded via an EPSRC PhD+ fellowship (EP/J500483/1); MM is grateful for the award of a Marie Curie fellowship funded by the ACRITAS FP7 initial training network (www.acritas.eu) under the Marie Skłodowska-Curie Actions, project reference ACRITAS-317348-Ares(2016) 909492. MM also thanks John Randall, James Owen and colleagues at Zyvex Labs (Richardson, Texas) for hosting a month-long secondment during which he gained valuable insights into automated scanning probe lithography of H:Si(100) surfaces. A significant amount of the research was also funded by the the European Commission’s FP7 ICTFET programme via the Atomic Scale and Single Molecule Logic gate Technologies (AtMol) project, Contract No. 270028. SPJ was funded via a Leverhulme Trust Early Career Fellowship, ECF-2015-005.

References

- [1] Lyding J W, Shen T-C, Hubacek J S, Tucker J R and Abeln G C 1994 Nanoscale patterning and oxidation of H-passivated Si(100)- 2×1 surfaces with an ultrahigh

- vacuum scanning tunneling microscope *Appl. Phys. Lett.* **64** 2010–2
- [2] Shen T-C, Wang C, Abeln G C, Tucker J R, Lyding J W, Avouris Ph and Walkup R E 1995 Atomic-scale desorption through electronic and vibrational excitation mechanisms *Science* **268** 1590–2
- [3] Foley E T, Kam A F, Lyding J W and Avouris Ph 1998 Cryogenic UHV-STM study of hydrogen and deuterium desorption from Si(100) *Phys. Rev. Lett.* **80** 1336–9
- [4] Soukiassian L, Mayne A J, Carbone M and Dujardin G 2003 Atomic wire fabrication by STM induced hydrogen desorption *Surf. Sci.* **528** 121–6
- [5] Hersam M C, Guisinger N P and Lyding J W 2000 Silicon-based molecular nanotechnology *Nanotechnology* **11** 70–6
- [6] Fuechsle M, Mahapatra S, Zwanenburg F A, Friesen M, Eriksson M A and Simmons M Y 2010 Spectroscopy of few-electron single-crystal quantum dots *Nat. Nanotechnol.* **5** 502–5
- [7] Haider M B, Pitters J L, DiLabio G A, Livadaru L and Wolkow R A 2008 Controlled coupling and occupation of silicon atomic quantum dots at room temperature *Phys. Rev. Lett.* **102** 046805
- [8] Weber B et al 2012 Ohm's law survives to the atomic scale *Science* **335** 64–7
- [9] Fuechsle M, Miwa J A, Mahapatra S, Ryu H, Lee S, Warschkow O, Hollenberg L C L, Klimeck G and Simmons M Y 2012 A single-atom transistor *Nat. Nanotechnol.* **7** 242–6
- [10] Schofield S R, Studer P, Hirjibehedin C F, Curson N J, Aeppli G and Bowler D R 2013 Quantum engineering at the silicon surface using dangling bonds *Nat. Commun.* **4** 1649
- [11] Ballard J B, Sisson T W, Owen I J H G, Owen W R, Fuchs E, Alexander J, Randall J N and Ehr J R V 2013 Multimode hydrogen depassivation lithography: a method for optimizing atomically precise write times *J. Vac. Sci. Technol. B* **31** 06FC01
- [12] Stokbro K, Thirstrup C, Sakurai M, Quaade U, Hu B Y-K, Perez-Murano F and Grey F 1998 STM-induced hydrogen desorption via a hole resonance *Phys. Rev. Lett.* **80** 2618–21
- [13] Thirstrup C, Sakurai M, Nakayama T and Stokbro K 1999 Temperature suppression of STM-induced desorption of hydrogen on Si(100) surfaces *Surf. Sci.* **424** L329–34
- [14] Shen T-C and Avouris Ph 1997 Electron stimulated desorption induced by the scanning tunneling microscope *Surf. Sci.* **390** 35–44
- [15] Avouris Ph, Walkup R E, Rossi A R, Akpati H C, Nordlander P, Shen T-C, Abeln G C and Lyding J W 1996 Breaking individual chemical bonds via STM-induced excitations *Surf. Sci.* **363** 368–77
- [16] Soukiassian L, Mayne A J, Carbone M and Dujardin G 2003 Atomic-scale desorption of H atoms from the Si(100)-2 × 1: H surface: inelastic electron interactions *Phys. Rev. B* **68** 035303
- [17] Tong X and Walkow R A 2006 Electron-induced H atom desorption patterns created with a scanning tunneling microscope: Implications for controlled atomic-scale patterning on H-Si(100) *Surf. Sci. Lett.* **600** L199–203
- [18] Boland J 1990 Structure of the H-saturated Si(100) surface *Phys. Rev. Lett.* **65** 3325–8
- [19] Boland J 1993 Scanning tunnelling microscopy of the interaction of hydrogen with silicon surfaces *Adv. Phys.* **42** 129–71
- [20] Dürr M and Höfer U 2006 Dissociative adsorption of molecular hydrogen on silicon surfaces *Surf. Sci. Rep.* **61** 465–526
- [21] Raza H 2007 Theoretical study of isolated dangling bonds, dangling bond wires, and dangling bond clusters on a H:Si(001)-(2 × 1) surface *Phys. Rev. B* **76** 045308
- [22] Chen S, Xu H, Goh K E J, Liu L and Randall J N 2012 Patterning of sub-1 nm dangling-bond lines with atomic precision alignment on H:Si(100) surface at room temperature *Nanotechnology* **23** 275301
- [23] Jarvis S, Sweetman A, Bamidele J, Kantorovich L and Moriarty P 2012 Role of orbital overlap in atomic manipulation *Phys. Rev. B* **85** 235305
- [24] Yurtsever A, Sugimoto Y, Tanaka H, Abe M, Morita S, Ondráček M, Puro P, Pérez R and Jelinek P 2013 Force mapping on a partially H-covered Si(111)-(7 × 7) surface: influence of tip and surface reactivity *Phys. Rev. B* **87** 155403
- [25] Štich I, Tóbiš J, Pérez R, Terakura K and Ke S H 2000 Tip-surface interactions in noncontact atomic force microscopy on reactive surfaces *Prog. Surf. Sci.* **64** 179–91
- [26] Ballard J B et al 2014 Pattern transfer of hydrogen depassivation lithography patterns into silicon with atomically traceable placement and size control *J. Vac. Sci. Technol. B* **32** 041804
- [27] Rahe P, Schütte J, Schniederberend W, Reichling M, Abe M, Sugimoto Y and Kühnle A 2011 Flexible drift-compensation system for precise 3D force mapping in severe drift environments *Rev. Sci. Instr.* **82** 063704
- [28] Dubois M, Perdigão L, Delerue C, Allan G, Grandidier B, Deresmes D and Stiévenard D 2005 Scanning tunneling microscopy and spectroscopy of reconstructed Si(100) surfaces *Phys. Rev. B* **71** 165322
- [29] Perdigão L, Deresmes D, Grandidier B, Dubois M, Delerue C, Allan G and Stiévenard D 2004 Semiconducting Surface Reconstructions of p-type Si(100) substrates at 5 K *Phys. Rev. Lett.* **92** 216101
- [30] Suwa Y, Matsuura S, Mujimori M, Heike S, Onogi T, Kajiyama H, Hitosugi T, Kitazawa K, Uda T and Hashizume T 2003 Dopant-pair structures segregated on a hydrogen-terminated Si(100) surface *Phys. Rev. Lett.* **90** 156101
- [31] Bellec A, Riedel D and Dujardin G 2008 Dihydride dimer on the Si(100): H surface studied by low-temperature scanning tunneling microscopy *Phys. Rev. B* **78** 165302